



3D porous catalysts for Plasma-Catalytic dry reforming of Methane: How does the pore size affect the Plasma-Catalytic Performance?

Jinxin Wang^{a,b}, Kaimin Zhang^b, Annemie Bogaerts^{a,*}, Vera Meynen^{b,c,*}

^a Plasma Lab for Applications in Sustainability and Medicine - ANTwerp, Department of Chemistry, University of Antwerp, Universiteitsplein 1, 2610 Wilrijk, Antwerp, Belgium

^b Laboratory of Adsorption and Catalysis, Department of Chemistry, University of Antwerp, Universiteitsplein 1, 2610 Wilrijk, Antwerp, Belgium

^c Flemish Institute for technological research, VITO NV, Boeretang 200, 2400 Mol, Belgium

ARTICLE INFO

Keywords:

Plasma catalysis
Dry reforming
3D porous catalysts
Effect of pore size
Dielectric barrier discharge reactor

ABSTRACT

The effect of pore size on plasma catalysis is crucial but still unclear. Studies have shown plasma cannot enter micropores and mesopores, so catalysts for traditional thermocatalysis may not fit plasma catalysis. Here, 3D porous Cu and CuO with different pore sizes were prepared using uniform silica particles (10–2000 nm) as templates, and compared in plasma-catalytic dry reforming. In most cases, the smaller the pore size, the higher the conversion of CH₄ and CO₂. Large pores reachable by more electrons did not improve the reaction efficiency. We attribute this to the small surface area and large crystallite size, as indicated by N₂-sorption, mercury intrusion and XRD. While the smaller pores might not be reachable by electrons, due to the sheath formed in front of them, as predicted by modeling, they can still be reached by radicals formed in the plasma, and ions can even be attracted into these pores. An exception are the samples synthesized from 1 μm silica, which show better performance. We believe this is due to the electric field enhancement for pore sizes close to the Debye length. The performances of CuO and Cu with different pore sizes can provide references for future research on oxide supports and metal components of plasma catalysts.

1. Introduction

Plasma catalysis is considered a promising alternative to various traditional chemical processes, such as the decomposition of gaseous pollutants and the synthesis of organic chemicals [1–3]. CO₂ reforming of methane (dry reforming) is one of the attractive processes among them since it simultaneously utilizes two greenhouse gases (CH₄ and CO₂), which can come from sustainable resources such as biogas, to produce fuels and chemical products [4–9]. Due to the low chemical reactivity of CH₄ and CO₂, the classical thermocatalytic reaction requires a high temperature (at least 800 °C) to provide sufficient energy to activate them, which leads to problems like energy loss and deactivation of the catalysts [10–15]. These problems can be overcome by non-equilibrium plasma, since it allows the reaction to proceed at relatively low temperatures (lower than 250 °C) [16–18]. The high-energy electrons produced by plasma can break the stable chemical bonds of CH₄ and CO₂, while the gas molecules themselves can remain close to room temperature, hence the term “non-equilibrium plasma” [19–21]. A popular type of non-equilibrium plasma reactor is the

dielectric barrier discharge (DBD) reactor, which is straightforward to be combined with a catalyst. Moreover, it is easily to be applied in the chemical industry because it can be operated at ambient temperature and atmospheric pressure [22–26].

A DBD reactor operating in CO₂/CH₄ mixtures is typically in filamentary discharge mode, composed of a large number of independent micro-discharge filaments, which is greatly affected by the size and geometry of the reactor, as well as by the packing materials and catalysts filled in the reactor [27–30]. Therefore, the interaction between the plasma and the catalyst must be taken into account to study the plasma-catalytic dry reforming, not only the reaction process of feed gas molecules and the catalyst. Moreover, the reactant gas in the plasma state may exhibit quite different properties than in thermal reactions. Hence, the role played by the catalysts is more complicated than in thermal catalysis and is still not entirely clear.

The catalysts used in the existing studies are often the same as or slightly modified from the catalysts for traditional thermocatalytic dry reforming. Some studies reported that the catalyst had a synergistic effect with the plasma to promote the conversion of CH₄ and CO₂. For

* Corresponding authors.

E-mail addresses: annemie.bogaerts@uantwerpen.be (A. Bogaerts), vera.meynen@uantwerpen.be (V. Meynen).

example, Vakili et al. [31] deposited Pt nanoparticles on the metal–organic framework material UiO-67 MOF as a catalyst, which enhanced the conversion of CH₄ and CO₂ in the diluted feed gases (5000 ppm). Zeng et al. [32] studied γ -Al₂O₃ supported transition metals (Ni, Mn, Co, Cu), and found that compared with only plasma in an empty reactor, filling pure γ -Al₂O₃ or γ -Al₂O₃ supported transition metal catalysts in the reactor yielded an improvement in the conversion of CH₄ (maximum increase was from ~ 14% to ~ 20%), although the conversion of CO₂ slightly decreased (from ~ 10% to ~ 9%). However, more studies showed inverse effects of the catalysts on plasma dry reforming, especially for those experiments using undiluted feed gases [33,34]. Wang et al. [18] also used a γ -Al₂O₃ support loaded with the same transition metal Cu as Zeng et al.. Moreover, also noble metals (Au, Pt), which are generally considered to be more active for dry reforming, were used as active ingredients [18,35]. However, due to the inhibition of the discharge by the catalysts, both the γ -Al₂O₃ with and without supporting metals reduced the conversion of CH₄ and CO₂ compared to the plasma reaction in an empty reactor, although the selectivity of some products was improved. Michielsen et al. [36] and Andersen et al. [37] reported that if keeping the same space time as the empty DBD reactor, packing materials and catalysts do have positive effects on the dry reforming (DRM) reaction. However, the (catalytic) packing material decreased the discharge volume in the reactor, leading to a shorter space time in the plasma. For some materials, the promotion of the DRM reaction due to the catalytic activity or electric field enhancement of the packing could not compensate for the decreased conversion caused by the loss in volume. In short, since there are so many factors affecting the interaction between catalyst and plasma, a wide variety of very different research results on plasma-catalytic dry reforming have been published in literature, even for similar packing materials. However, a general observation is that the majority of porous catalysts did not show an improvement in plasma catalysis [38].

In order to study how porous materials affect the plasma in a DBD reactor, some researchers have simulated the behavior of plasma streamers in catalyst pores. Zhang et al. [39–42] studied by modeling whether plasma can enter catalyst pores. Their simulations showed that plasma could only be generated or penetrate into pores that are larger than the so-called Debye length, which is hundreds of nanometers at typical plasma-catalytic conditions. However, the porous materials applied as catalyst supports in the existing plasma-catalytic dry reforming studies were usually only with micropores or mesopores smaller than 10 nm. Hence, these are much smaller than the pore size in which plasma can be formed. Although microporous or mesoporous materials show good performance in traditional thermocatalytic dry reforming, because of their large specific surface area, the surface area resulting from the small pores might be ineffective for plasma reactions according to the simulation of Zhang et al. However, if the micropores and mesopores were ineffective for plasma reactions, the question arises what then caused the improved conversion in plasma-catalytic dry reforming, reported in those papers applying microporous or mesoporous catalysts?

In many papers, only part of the DBD reactor space was packed with a little catalyst, to promote conversion of dry reforming by catalysts, although they might not mention or study this [32,43,44]. Tu et al. reported that instead of packing the catalyst particles into the entire discharge gap, packing a small amount of catalyst into a part of the gap improved the conversion of dry reforming [38]. Ray et al. studied the performance of Ni-Mn/ γ -Al₂O₃ bimetallic catalyst for dry reforming, and found that the reactant conversion of full catalyst packing and 50% catalyst packing in a DBD reactor were similar to or even worse than that without catalyst, while 25% catalyst packing showed the best performance among all conditions [45]. They suggested that the reduction of discharge in DBD reactors, resulting from catalyst particle packing, is the reason that a partially packed or empty reactor has better performance than a full catalyst packed one. Furthermore, the conclusion of Zhang et al. [39–42] that the plasma cannot enter or be formed in the pores of

microporous or mesoporous materials (e.g. γ -Al₂O₃) is another reason that a catalyst packing greatly reduces the plasma volume. It is reasonable that the more catalyst filling, the greater the negative effect on the plasma reaction. However, the dry reforming performance of some partially packed reactor (e.g. 25% Ni-Mn/ γ -Al₂O₃ packing) is better than that of an empty reactor, which implies that the catalyst also has a positive effect on the plasma dry reforming in some way, even if the pores are unreachable to plasma. There is a balance between this positive effect and the negative effect of catalyst packing, which is the reason for the better conversion in partially packed reactors. However, this partial packing method is a compromise between catalyst and plasma. It reduces the negative effect of catalyst on the plasma, but also means that neither the plasma nor the catalyst can be fully utilized. Since one of the negative effects of catalysts on plasma is caused by the small pore size, a potential way is to apply catalysts with larger pores into which the plasma can enter, to see if it can maintain the positive effects of the catalysts while decreasing the negative effects of catalyst particles on plasma discharge. In addition, although the micropores and mesopores are ineffective for plasma discharge, their comprehensive effects on the plasma dry reforming processes are unknown. In order to truly combine the advantages of the catalyst and plasma reaction, and to know the right future research direction of the catalyst for plasma reactions, it is crucial to study the role of catalyst pores and the effect of pore size in plasma-catalytic dry reforming.

Some studies compared different catalyst supports that may possess different pore sizes, but they were limited to materials with pores of a few nanometers, while the larger plasma-reachable pores have rarely been studied [46–48]. Moreover, since the difference in materials, structures and properties of different supports resulted in too many interference factors, it is impossible to conclude the effect of the pore size on plasma dry reforming from these studies.

In the present paper, we thus synthesized catalysts of the same material with different pore sizes in the range of a few nanometers to micrometers and studied their performance for dry reforming in a DBD plasma reactor. Since the common porous supports or porous structure preparation process cannot adjust the pore sizes in such a large span, silica spheres with different diameters were prepared first as templates and then removed by etching to get 3D porous catalysts with different and controlled intraparticle pore sizes, as shown in Fig. 1. The size of interparticle voids resulting from particle packing is not the focus of this work and did not vary significantly between samples. In existing studies, various metals, such as Pt, Au, Rh, Ru, Cu, Ni, etc., are typical active components of plasma dry reforming catalysis [18,37,45,49]. Noble metals usually have higher catalytic activity, but considering the cost of these catalysts and their presence on the critical raw material list, more abundant metals such as Cu and Ni are more promising research targets. In this work, copper was applied as the metal active ingredient, and unreduced copper oxide was also investigated as an example of a material with a certain dielectric constant. The porous structured samples consisted of pure copper or copper oxide without any support, so the influences of the supports (e.g. metal-support effects, alkalinity of the supports) do not have to be considered in this study, in contrast to literature studies using porous supported catalysts.

2. Experimental

2.1. Preparation of the 3D porous catalysts

Ammonia solution (wt % = 25 %), tetraethyl orthosilicate (TEOS) and ethanol were purchased from Sigma-Aldrich. Copper nitrate trihydrate was purchased from Acros.

2.1.1. Preparation of SiO₂ spheres template

The silica spheres were synthesized by a modified Stöber method from our previous study [50]. A certain amount of ammonia solution was dissolved in deionized water. The solution was agitated gently at

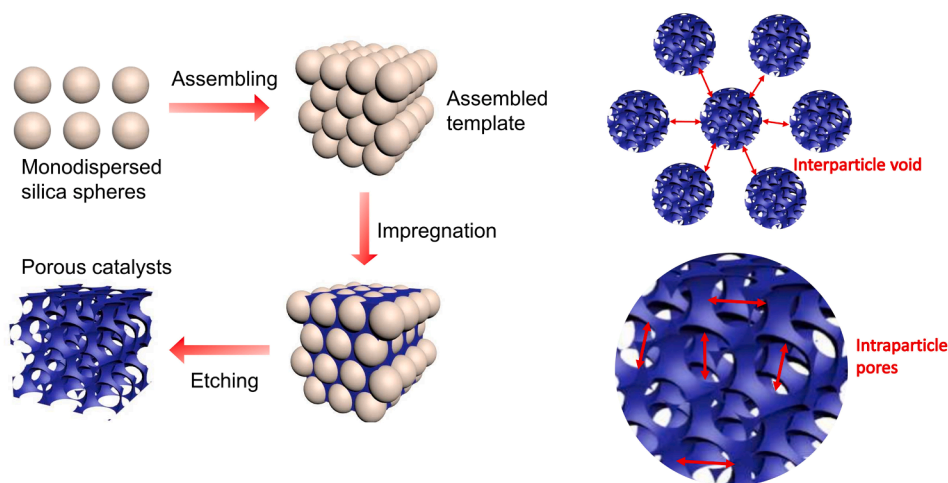


Fig. 1. The process for the 3D porous catalysts synthesis (left), and explanation of the interparticle voids and intraparticle pores (right).

20 °C and 200 mL tetraethyl orthosilicate was added into it. Then, we kept stirring the mixture at the same temperature for 24 h. The silica spheres were obtained after centrifugation and drying at 80 °C for 24 h. The different ratios of ammonia to water were used to adjust the diameter of the silica spheres. Silica particles with diameters of about 10 nm, 50 nm, 100 nm, 600 nm, 1 and 2 μm were synthesized as templates for the next step of impregnation.

2.1.2. Impregnation and etching of metal ingredients

The silica samples were calcined at 800 °C for 12 h to interconnect the spheres. Excess copper nitrate (twice the mass of silica) was dissolved in ethanol and subsequently the silica was added. The mixture was left without agitation for 48 h to complete the impregnation. Then, the solid product was dried in an oven at 80 °C for 24 h. The resulting sample was calcined in a crucible at 650 °C to decompose the nitrate species. Finally, the silica template was removed by etching with 2 M NaOH aqueous solution at 80 °C for 5 h. After washing to neutral and drying at 80 °C, the 3D porous metal oxide was obtained.

The samples were denoted by the diameter of the silica particles used in the impregnation. For example, copper oxide synthesized using 10 nm and 2.5 μm silica particles as templates were denoted as CuO-10 and CuO-2500, respectively, and if reduced with H_2 before plasma testing, the catalysts are denoted as Cu-10 and Cu-2500, respectively.

2.2. Characterization of the catalysts

X-ray powder diffraction (XRD) was applied to characterize the crystal phases of all the CuO samples. The measurements were performed by a D8 advance Eco diffractometer with Cu-K α radiation ($\lambda = 1.5406 \text{ \AA}$) at a scanning range of 10–80° 2 θ and a scanning rate of 0.04°/4 s. The XRD patterns of all the samples were normalized by dividing every peak by the most intense peak to get relative intensities.

The scanning electron microscopy (SEM) and energy dispersive X-ray spectroscopy (EDX) were used to investigate the topography and surface composition of the samples. They were carried out by the FEI Quanta ESEM FEG 250 field emission microscope with an EDX detector operating at 20 kV.

Nitrogen sorption was used to study the pore size (<50 nm) and specific surface area of the samples. The measurements were carried out on a Quantachrome Quadrasorb SI automated gas sorption system. The samples were degassed for 16 h under high vacuum at 200 °C before the N_2 -sorption measurements. The temperature was kept at -196 °C by liquid nitrogen during the N_2 -sorption. The surface area was determined by the multi-point Brunauer–Emmett–Teller (BET) method and the pore size distribution was determined by non-local density functional theory (NLDFT) on the adsorption branch.

Mercury porosimetry was applied to study the macropores (>50 nm). The mercury porosimetry was executed on a Thermo Electron Corporation Pascal 140 + 240 series, operating in 2 different pressure regimes. Prior to mercury intrusion the samples were vacuum dried for 10 min.

Diffuse reflectance infrared Fourier transform (DRIFT) spectrometry was performed with a resolution of 4 cm^{-1} and the accumulation of 100 scans, on a Nicolet 6700 Fourier Transform IR spectrometer, to study the surface groups of the CuO samples. The samples for the measurements were diluted by KBr to 0.5 wt%, and pure KBr was used as a background. The spectra were obtained after stabilizing for 30 min with 80 mL/min of Ar flushing at room temperature.

Hydrogen-temperature programmed reduction (H_2 -TPR) and oxygen-temperature programmed oxidation (O_2 -TPO) were combined to check if the CuO samples were reduced completely in the tube furnace when Cu was needed for the dry reforming test. The measurements were carried out on the ChemStar TPX Chemisorption Analyzer. First, the samples were degassed at 350 °C for 2 h with 50 mL/min pure He flushing. After cooling down to 50 °C, the first O_2 -TPO was carried out from 50 °C to 800 °C with 10 °C/min ramping rate, under 5% O_2/He at a flow rate of 50 mL/min. After cooling down to 50 °C again, the H_2 -TPR was performed to 800 °C with 10 °C/min ramping rate, under 50 mL/min of 5% H_2/Ar . The second O_2 -TPO was done with the same procedure as the first one after cooling down.

Thermogravimetric analyses (TGA) were performed on a Mettler Toledo TGA-DSC 3 + in a continuous 80 mL/min flow of O_2 . A heating rate of 10 °C/min from 30 °C to 800 °C was applied.

2.3. Plasma-catalytic performance test of the catalysts

2.3.1. Set-up of the DBD reactor

A fixed bed DBD reactor as illustrated in Fig. 2 was applied to study the plasma-catalytic performance for dry reforming of the catalysts with different pore sizes. The inner electrode was a stainless steel rod with outer diameter of 13 mm. An alumina dielectric tube with 21.8 mm outer diameter and 17.41 mm inner diameter was coaxially placed over the stainless steel rod as a dielectric barrier, so the discharge gap between the inner electrode and dielectric barrier was about 2.2 mm. A stainless steel mesh was used as outer electrode by tightly winding it on the outside of the alumina tube. The length of the outer electrode, which determines the length of the discharge zone, was 10 mm. 4 g of catalyst powder was filled in the whole plasma zone with 2 g glass wool at both sides to fix the powder. The tapped volume of 4 g of samples was larger than the volume of the discharge space (1.05 mL), to avoid the possible effect of glass wool on both sides on the discharge. Moreover, in order to measure the weight filled in the discharge space to calculate the packing density, the particles were repacked in an amount that just fills the

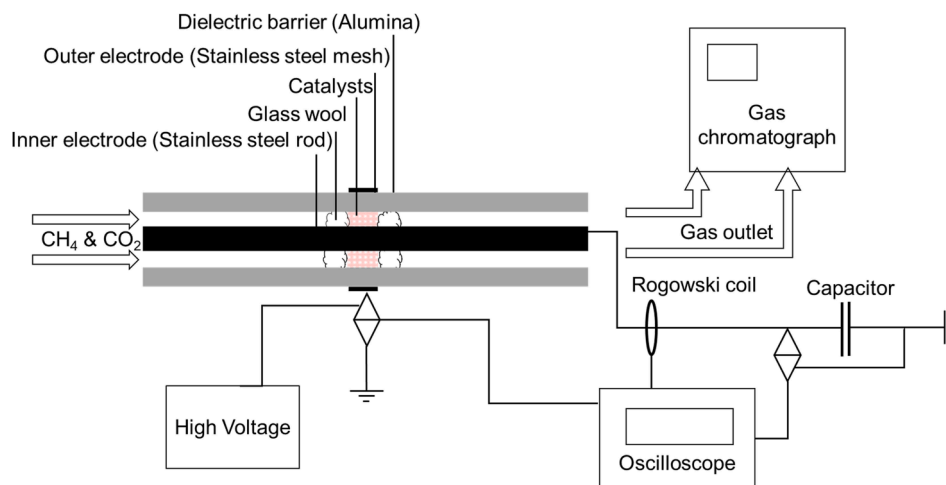


Fig. 2. DBD reactor setup for the dry reforming of methane.

discharge space of the reactor.

The inner electrode was grounded, and the outer electrode was connected to a high voltage supplied by a function generator (Tektronix, AFG 2021) and a high voltage amplifier (TREK, Model 20/20C-HS). The generator provided a signal with a frequency of 3000 Hz, and the amplifier amplified the input signal by 2000. A high-voltage probe (Tektronix, P6015A) was used to measure the voltage, and a Rogowski coil (Pearson 4100) was used to monitor the current. The current profile was filtered by applying a Savitzky-Golay filter of polynomial order 3 to exclude the signal noise [28]. The number of peaks per period in the current profile, after excluding signal noise, was used to study the number of micro-discharges in this study. It should be noted that this is not the exact number of discharges that occurred in the reactor, since the discharges might have occurred simultaneously, while only one peak of current was shown in the current profiles. In addition, some small discharges might be excluded as signal noise. However, multiple collections of current data and an average value of the number of current peaks can be used to compare and study the effects of different samples on the discharge even though the obtained numbers should not be interpreted as absolute but as apparent values. The charge in the plasma was monitored by a capacitor (10 nF) connected in series and a low-voltage probe (Picotech, TA150) connected in parallel with it. The displaced charge was obtained from it by taking the detected charge difference before and after discharge. All the signals were collected by an oscilloscope (Picotech, Picoscope 6402D) and shown on a PC. The data was calculated in real time to adjust the amplitude of the input signal from the amplifier, in order to keep the power of the power supply constant at 50 W. The calculation and counting of electrical parameters are done automatically by a MATLAB script.

2.3.2. Catalyst performance evaluation

The copper oxide was filled and tested directly in the reactor. However, to evaluate the copper samples, the copper oxide powder was reduced in a tube furnace (Carbolite Gero TF1 12/60/300) with 250 mL/min of 2% H₂/Ar gas flow at 450 °C for 8 h before being packed into the reactor. The reduction temperature of CuO was 450 °C which is determined by H₂-TPR.

For the plasma-catalytic dry reforming test, the feed gas consisted of 5 mL/min of CH₄ and 5 mL/min of CO₂, and the flow rate was controlled by mass flow controllers (Bronkhorst EL-FLOW Select). 10 mL/min of N₂ was added in the outlet gas as internal standard to exclude the impact of the gas expansion. The product gases from the reactor outlet were analyzed by an online gas chromatograph (Trace GC 1310, Interscience) equipped with a thermal conductivity detector (TCD) and a flame ionization detector (FID). Thermocouples were used to measure the

temperature of the external electrodes and the gas at the outlet (about 10 cm from the discharge space) of the reactor. In all our experiments, the gas temperature at the outlet of the reactor was about 20–25 °C, and the temperature of the external electrode was about 50 °C. Also, Van Turnhout et al. recently presented a novel method to determine the temperature of the catalyst surface, and revealed that the plasma-induced temperature rise in a DBD reactor is limited (≤ 150 °C) [51]. It might always be possible that the temperature in the reactor is higher at some places (local hot spots) and dependent on the type of packing material and operating conditions; however, since thermal dry reforming hardly takes place below 300 °C [38], we can consider that the conversion of CH₄ and CO₂ in our reactor is mainly due to the plasma reaction. After flushing the filled reactor with the feed gas for 30 min without plasma, the composition of the outlet gas was analyzed and recorded as blank measurements, and the amount of CO₂ and CH₄ were denoted as CO_{2,in} and CH_{4,in} respectively. Then, the power was applied to generate plasma, and kept at 50 W for 30 min. The gases generated and unconverted feed gas after 30 min were analyzed and their amounts were marked with “out”, i.e., CO_{2,out}, CH_{4,out}, H_{2,out}, CO_{out} and C_xH_yO_{z,out}. The conversion of CO₂ and CH₄ are calculated by Eq. (1) and Eq. (2)

$$X_{\text{CO}_2} = \frac{\text{CO}_{2,\text{in}} - \text{CO}_{2,\text{out}}}{\text{CO}_{2,\text{in}}} \hat{A} \cdot 100\% \quad (1)$$

$$X_{\text{CH}_4} = \frac{\text{CH}_{4,\text{in}} - \text{CH}_{4,\text{out}}}{\text{CH}_{4,\text{in}}} \hat{A} \cdot 100\% \quad (2)$$

The selectivity (S) of the products are defined by Eq. (3) to Eq. (5)

$$S_{\text{H}_2} = \frac{\text{H}_{2,\text{out}}}{2 \times (\text{CH}_{4,\text{in}} - \text{CH}_{4,\text{out}})} \hat{A} \cdot 100\% \quad (3)$$

$$S_{\text{CO}} = \frac{\text{CO}_{\text{out}}}{(\text{CH}_{4,\text{in}} - \text{CH}_{4,\text{out}}) + (\text{CO}_{2,\text{in}} - \text{CO}_{2,\text{out}})} \hat{A} \cdot 100\% \quad (4)$$

$$S_{\text{C}_x\text{H}_y\text{O}_z} = \frac{x \times \text{C}_x\text{H}_y\text{O}_{z,\text{out}}}{(\text{CH}_{4,\text{in}} - \text{CH}_{4,\text{out}}) + (\text{CO}_{2,\text{in}} - \text{CO}_{2,\text{out}})} \hat{A} \cdot 100\% \quad (5)$$

The energy yield (EY) of the reaction was defined as the amount of CO₂ and CH₄ that can be converted per kJ of input energy, as shown in Eq. (6)

$$\text{EY (mmol/kJ)} = \frac{(V_{\text{CO}_2} X_{\text{CO}_2} + V_{\text{CH}_4} X_{\text{CO}_4})}{P V_m} \hat{A} \cdot \frac{1000}{60} \left(\frac{\text{Wmin}}{\text{kJ}} \right) \quad (6)$$

where V_{CO_2} and V_{CH_4} are the volumetric flow rate (in mL/min) of CO₂ and CH₄ in the feed gas. V_m is the molar gas volume (24.4 mL/mmol) and P is the plasma power (in W). The factor 1000/60 (Wmin/kJ) is to

convert the unit from Wmin to kJ.

The DRM reaction produces CO, H₂ and various hydrocarbon products, resulting in the expansion with an unknown coefficient and pressure rise of the outlet gases. The GC always depressurizes the gases to ambient pressure during sampling, so the direct calculation of conversion and selectivity from gas_{out} and gas_{in} obtained by the GC will have systematic errors. Therefore, 10 mL/min N₂ flow was applied as the internal standard to reduce the errors [52].

3. Results and discussion

3.1. Structure and properties of the catalysts

The normalized XRD patterns of the 3D porous CuO samples, synthesized from silica particles of different sizes, are shown in Fig. 3, and the original XRD patterns are shown in Fig. S1 in Supplementary Material. A sample with copper oxide loading but without etching away the SiO₂ is also characterized by XRD for comparison. It is obvious that a broad peak attributed to (111) reflection of SiO₂ is detected at $2\theta = 21.60^\circ$ in the sample without etching, while it is no longer present in all etched porous copper oxide samples. The diffraction peaks at other angles, such as the peaks at $2\theta = 32.51^\circ, 35.42^\circ, 38.71^\circ, 48.72^\circ, 53.49^\circ, 61.52^\circ, 66.22^\circ, 68.12^\circ, 72.37^\circ,$ and 74.98° are indexed to the (110), (002), (111), (20-2), (020), (11-3), (31-1), (220), (311), and (004) crystal planes of Tenorite CuO (JCPDS 48-1548). These peaks get sharper with the increase of particle size of the applied SiO₂ template during the syntheses (from CuO-10 to CuO-600), suggesting that the crystallinity and crystallite size of CuO is getting higher owing to the CuO sintering by calcination at 650 °C. When smaller silica particles are used as templates, the gaps between the particles are smaller, which restricts the growth of crystallites, resulting in smaller grains of copper oxide and thinner pore walls. On the contrary, thicker pore walls and larger copper oxide crystallites are obtained when larger silica particles are used as templates. The crystallinity and crystallite size of the CuO-600, CuO-1000 and CuO-2000 is similar, and no longer increase significantly with increasing particle size of the SiO₂ template.

SEM measurements were carried out to observe the morphology and pore sizes of the 3D porous CuO samples, and the images are shown in Fig. 4. All the samples in the figure show spherical pores with relatively uniform size. According to the design of the synthesis process shown in Fig. 1, the pores should be connected, and the holes in the pore walls observed in Fig. 4 fit that. EDX analysis proves that the silica particles

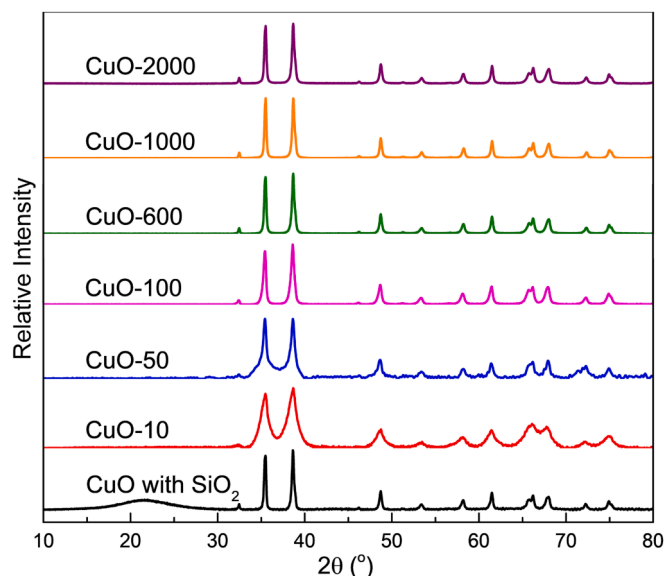


Fig. 3. The normalized XRD patterns of the 3D porous CuO samples.

can be etched away successfully by NaOH solution (see Table S1 in Supplementary Material) as <0.5% Si is left on the surface of CuO. 30 measurable pores in the SEM images were measured to get the average pore size of the samples, and it was found that the pore size of the samples were slightly smaller than the diameter of the corresponding silica particle templates used in the synthesis. The mean diameter of CuO-100, CuO-600, CuO-1000 and CuO-2000 are about 82 nm, 574 nm, 937 nm, and 1891 nm, respectively. The smaller diameter is probably caused by shrinkage of the pores during the calcination at 650 °C and/or the etching of silica spheres. The pore size of CuO synthesized from 10 nm and 50 nm silica particles were too small to be observed by scanning microscopy, but their pore size can be characterized and calculated by N₂-sorption, by which more comprehensive pore diameter data of the samples can be obtained, including information of the bulk of the pores (adsorption branch) and the pore necks (desorption branch). A closer look inside the pores reveals that the junctions between the spherical pores (i.e. pore necks) are smaller in size than the diameter of the spherical pores themselves. This can be more clearly observed in the CuO SEM images of the larger pores. This is reasonable because the size of the contact surface between the template silica spheres was smaller than the diameter of the spheres themselves. The shape of the pores is a stack of multiple hollow spheres, rather than a cylindrical channel. The SEM images of CuO-100, CuO-600, CuO-1000 and CuO-2000 were only used to measure the diameter of the pore bodies, not the size of the pore necks. To measure the diameter of the pore necks more accurately, mercury intrusion porosimetry was applied.

Fig. 5 displays the pore size distribution of the porous copper oxide samples based on N₂-sorption (NLDFT adsorption branch) and mercury intrusion porosimetry. The pore size distribution (calculated by BJH desorption branch) and N₂-sorption isotherms of CuO-10 and CuO-50 are shown in Supplementary Material, Fig. S2 to obtain more complete information on the pore structure. Since nitrogen sorption and mercury intrusion porosimetry are applicable to different pore size ranges, the CuO-10 and CuO-50 samples were characterized by nitrogen sorption, and the other samples were determined by mercury intrusion porosimetry. Due to the different systematic errors of the two characterization methods, the pore size distribution of samples obtained by different methods cannot be accurately compared, but they are put into the same figure to roughly compare the pore size distributions and get an intuitive impression. Important to note is that, due to the ink-bottle effect, the pore size obtained by mercury intrusion is only the size of pore necks, which will be smaller than the actual bulk pore size (cf. SEM images, Fig. 4) of the samples [53,54], while the pore size obtained by N₂-sorption includes both pore neck size (desorption branch, Fig. S2) and bulk pore size (adsorption branch, Fig. 5). The pore size distribution of all samples suggests relatively uniform pores [53]. It is worth mentioning that because the synthesized CuO samples are powders with tens of μm particle size, there is another broad pore size distribution at the micrometer scale in the results of mercury intrusion (as shown in Fig. S3), which reflects the size of the inter-particle gaps rather than the bulk pore size [55,56].

The maxima of the pore size distributions calculated from N₂-sorption and mercury intrusion porosimetry of all CuO samples are listed in Table 1. For CuO-10 and CuO-50, the pore size is much smaller than the diameter of the silica spheres used in the synthesis, which might be caused by shrinkage during thermal treatments [57]. In addition, consistent with the conclusions drawn from the SEM images, the pore neck size of CuO-100, CuO-600, CuO-1000, and CuO-2000 measured by mercury intrusion is smaller than the diameter of the silica spheres used in the synthesis. Although the pore size of all porous samples is not equal to the diameter of the silica spheres, it is obvious that there is a positive correlation with it, resulting in an increasing trend with the use of larger silica template particles. Hence, uniform pore catalysts with different pore sizes are indeed successfully prepared over a large pore size span. The apparent surface area determined using the Brunauer–Emmett–Teller (BET) theory by N₂-sorption is also listed in Table 1. Initially, it

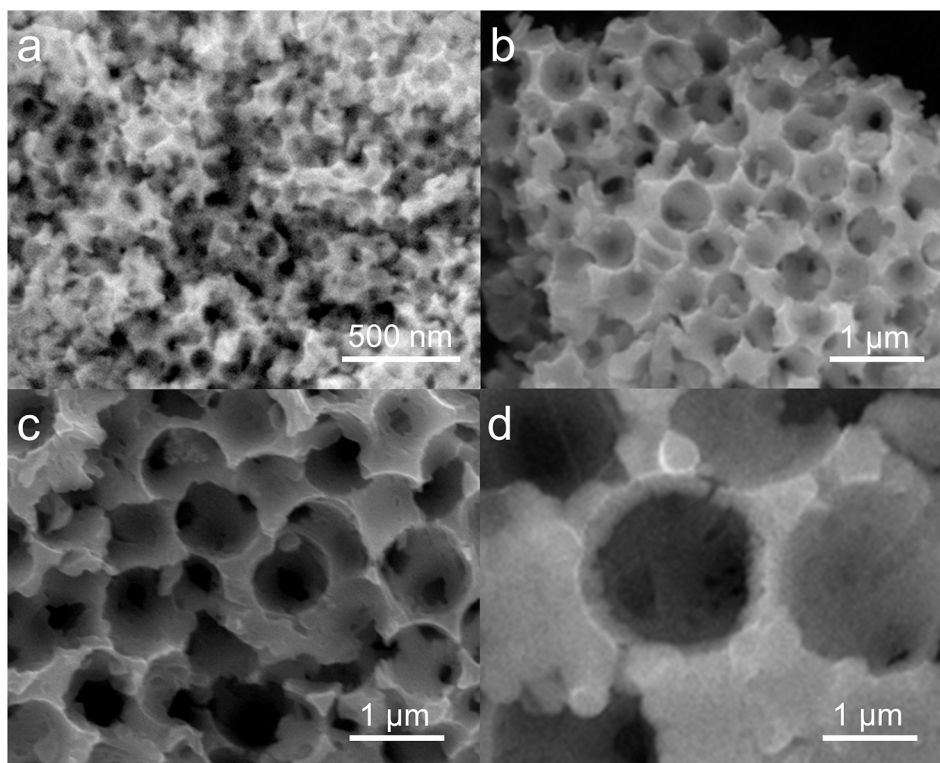


Fig. 4. SEM images of 3D porous CuO. (a) CuO-100 synthesized from silica particles with a diameter of about 100 nm. (b) CuO-600 synthesized from silica particles with a diameter of about 600 nm. (c) CuO-1000 synthesized from silica particles with a diameter of about 1 μm . (d) CuO-2000 synthesized from silica particles with a diameter of about 2 μm .

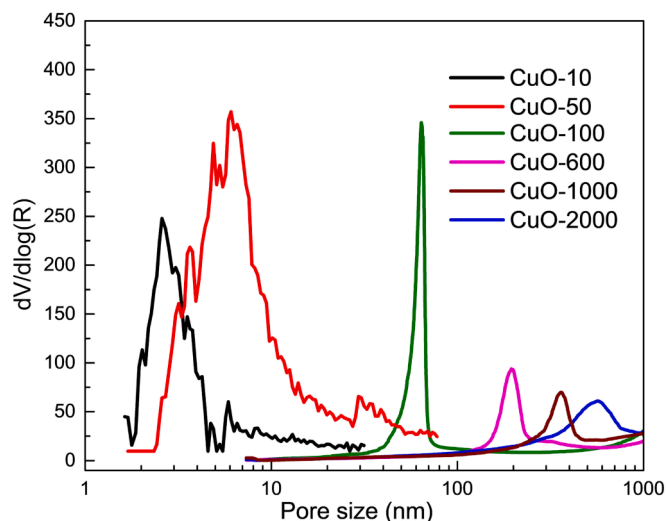


Fig. 5. Pore size distribution of 3D porous CuO samples obtained by N_2 -sorption (for CuO-10 and CuO-50) and mercury intrusion (for the other samples).

decreases rapidly with increasing pore size from CuO-10 to CuO-100. However, for the macroporous samples from CuO-100 to CuO-2000, the differences in specific surface area are very small as the pore size changes.

In addition, as shown in Fig. S4, the porous CuO particles synthesized by the method in this paper are not uniform in shape and particle size. The particle diameters of the porous CuO particles range from $\sim 5 \mu\text{m}$ to $\sim 40 \mu\text{m}$, and the average particle diameters calculated from measurements of more than 50 particles from the SEM images of Fig. S4 are summarized in Table 1. As shown in the table, compared with the large differences between the pore diameters (ranging from 2.6 to 1891 nm),

the difference in mean particle diameter between the sample particles was relatively small, and the particle diameter did not show an obvious tendency to increase with increasing pore size. The average particle diameter of CuO-10 and CuO-50 was slightly smaller than for the other samples, because they included more small particles around $5 \mu\text{m}$. Due to the similar mean particle diameters of the samples, their packing densities in the reactor, calculated from the weight of the particles packed in the discharge zone and the volume of the discharge space, as shown in Table 1, did not show significant variations with pore size. Therefore, samples with different pore sizes packed in the DBD reactor are expected to have similar space times. Hence, although the particle size and interparticle void space, as well as the packing density of the particles, could in principle affect the plasma performance and we cannot exclude it, its impact is expected to be less for all packing materials used in this work, compared to the change in pore size, which covers more than three orders of magnitude.

The infrared (IR) spectra of the CuO samples with different pore sizes are shown in Fig. S5. After flushing with 80 mL/min Ar for 30 min, all CuO samples did not show obvious hydroxyl groups, probably due to the 650°C calcination during the syntheses. The peaks appearing at around 537 cm^{-1} and 585 cm^{-1} can be attributed to the vibrations of Cu-O. A peak at 835 cm^{-1} could be assigned to the residual traces of silica after the etching, and no other peaks of SiO_2 was observed. A sample of CuO-1000 was characterized by IR again after the DRM, and no significant change on its surface properties was observed after plasma based dry reforming.

3.2. Dry reforming performance of the catalysts with different pore sizes

Plasma-catalytic dry reforming tests were performed on porous samples with different pore sizes before and after reduction. Fig. S6 shows the results of TPO-TPR-TPO of the samples after reduction. The oxygen consumption of the two TPOs was consistent, indicating that the CuO samples were completely reduced in the tube furnace. The

Table 1Pore sizes and specific surface areas of 3D porous CuO samples obtained from N₂-sorption, SEM and mercury intrusion.

Samples	Bulk pore diameter	Pore neck diameter	Specific surface area	Mean particle diameter ^d	Packing density	Packing density of reduced sample
CuO-10	2.6 nm ^a	/	236 m ² /g	8 μm	1.6 g/mL	1.7 g/mL
CuO-50	6.1 nm ^a	4.3 nm ^a	152 m ² /g	8 μm	1.7 g/mL	1.8 g/mL
CuO-100	82 nm ^b	64.0 nm ^c	8 m ² /g	10 μm	1.7 g/mL	1.7 g/mL
CuO-600	574 nm ^b	195.0 nm ^c	2 m ² /g	9 μm	1.6 g/mL	1.7 g/mL
CuO-1000	937 nm ^b	361.2 nm ^c	2 m ² /g	9 μm	1.6 g/mL	1.7 g/mL
CuO-2000	1891 nm ^b	565.6 nm ^c	1 m ² /g	10 μm	1.7 g/mL	1.8 g/mL

^a Pore size characterized by N₂-sorption, including bulk pore diameter (deduced by NLDFT from the adsorption branch) and pore necks diameter (deduced by BJH from the desorption branch). ^bBulk pore size measured and calculated by SEM images. ^cPore size characterized by mercury intrusion, which is considered to only account for the size of the pore necks. ^dThe particle distribution is broad (see the SEM images in Figure B.3), and thus the mean value is only present as a rough indication of differences in size between different powders but cannot be used to derive conclusion about e.g. void space due to the broad particle size distribution.

conversions of CH₄ and CO₂ in the plasma-catalytic reaction are shown in Fig. 6. The dashed lines in Fig. 6 are the CH₄ and CO₂ conversions at the same gas flow in an empty reactor only with plasma. In most cases, similar to the results in the majority of literature on plasma dry reforming, the CH₄ and CO₂ conversions for the catalysts were lower than those in the empty reactor at the same flow rate. This is because the positive effects of catalysts are not enough to compensate for their negative effects, such as hindering discharge and reducing space time. However, the best performing samples for a certain pore size in Cu and CuO (i.e. Cu-10 and CuO-1000) exhibited higher conversion than the empty reactor, illustrating the importance of the pore size effect on the plasma catalytic process, and the positive effects of the fully packing catalyst with suitable properties in the plasma catalytic dry reforming can cover its negative effects. There are very similar trends in Fig. 6a (reduced copper samples) and Fig. 6b (unreduced copper oxide samples). The first trend is that among the samples with pore sizes smaller than Cu-1000 or CuO-1000, the smaller the pore size, the higher the obtained conversion. This seems normal from a thermocatalytic dry reforming point of view, because the smaller pore catalysts have a higher surface area (see specific surface area of the different samples in Table 1) to facilitate the adsorption and catalytic reaction at the surface. In a plasma reaction, however, it is unusual. Previous studies on pore size generally suggested that the high surface area in small pores was ineffective since the smaller the pore size, the fewer electrons in the plasma can propagate into the pores during the discharge [39–41,58–61]. The direct comparison of the performance of catalysts with different pore sizes (Fig. 6) shows results that are in contrast to the conclusions drawn from previously reported simulations or experimental studies of plasma propagation within catalyst pores [40,41,59,60]. The results suggest that although electrons may not be able to enter the smaller pores to activate gas molecules and interact

with the catalyst surface inside the pores, the smaller pores still have some advantages, which are more important than the fact that plasma cannot enter inside these small pores.

First, the advantage of materials with large pores enabling more electrons to enter to react with the surface may not be as great. According to the data shown in Table 1, even if the pore size is large enough that the plasma streamer can propagate directly in it, resulting in the effective surface area of plasma reaction equal to its total surface area, the specific surface area of the catalyst with macropores is so low that it could not bring much benefit to the catalytic reaction. Second, although it is difficult for electrons in the plasma to enter the smaller pores to activate gas molecules due to the prevention of the plasma sheath, radicals or positively charged ions generated in the plasma will not be blocked. These plasma species may still diffuse into the pores, or (in case of the ions) even be accelerated out of the plasma into the pore, and thus react with the catalyst surface [61,62]. The lifetime of the free radicals will determine how deep they can penetrate into the pore. Third, the high roughness of the catalysts with small pores, resulting from the higher number of pores at the surface, causes electric field enhancement in the plasma, which creates more reactive plasma species that can interact with the catalyst. It can also be observed that the plasma power and the average filament charge show a correlation with the conversion of the reactants (we refer to Table 2 later for more details) [42,63–65]. Fourth, The larger external surface area of the catalysts with small pores (again due to a higher number of pores at the surface), may be another reason for their better performance. Fifth, the small crystallite size of catalysts with small pores shown in Fig. 3 may also be favorable for the plasma catalytic dry reforming, because the small crystallites have more exposed active sites [66–69]. Sixth, space time may also affect the conversion. As shown in Fig. S7, the conversion of CO₂ and CH₄ for two representative samples, i.e., Cu-10 and CuO-

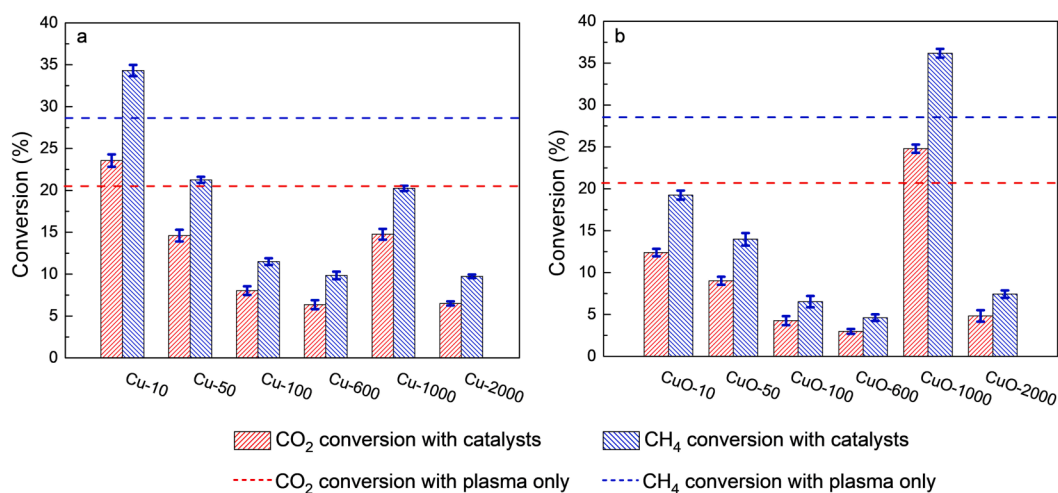


Fig. 6. Conversion of CH₄ and CO₂ in plasma-catalytic dry reforming, of 3D porous (a) Cu and (b) CuO samples with different pore sizes. The dashed line is the conversion of the empty reactor only with plasma at the same gas flow rate. The error bars were obtained from standard errors based on three repeat experiments.

Table 2

Electrical characterization data measured and calculated from the recorded signals of the oscilloscope of the DRM experiments with the samples of different pore sizes.

Samples	U _{pp} (kV)	Power supplied (W)	Plasma power (W)	Displaced charge (nC)	Number of micro-discharges (a.u./T)	Average filament charge (nC/disch.)
Empty reactor	25.9	50.5	27.8	/	176	/
Cu-10	26.3	50.5	19.5	558	141	4.2
Cu-50	28.3	50.2	15.7	596	137	3.8
Cu-100	26.7	50.2	16.5	529	168	3.3
Cu-600	27.3	50.2	16.5	561	154	3.2
Cu-1000	28.0	50.1	15.7	488	139	4.1
Cu-2000	26.6	50.3	17.2	562	165	3.8
CuO-10	26.9	50.4	20.1	547	138	4.0
CuO-50	26.7	49.9	19.3	557	156	3.6
CuO-100	26.4	50.3	19.7	671	134	5.0
CuO-600	26.4	50.3	19.2	665	155	4.3
CuO-1000	26.0	50.6	24.4	608	85	7.2
CuO-2000	26.8	50.5	19.5	589	151	3.9

1000, is greatly affected by the gas flow rate (which results in different space times). It should be realized that small variation in space time resulting from packing density variation can also affect the performance results to some extent. Moreover, as mentioned before, the CuO-10 and CuO-50 particles had slightly (10–20%) smaller mean particle diameters (8 μm versus 9–10 μm). The void space between the particles and the contact points between particles might be different. This provides a complexity of positive and negative effects of performance, which are mutually interfering and are expected to have an optimum value of particle size [27,28]. However, since the differences in mean particle diameter and packing densities between the samples were small (compared to the 3 orders of magnitude differences in pore sizes) and did not show an obvious trend with pore size, it is difficult to estimate the role of space times, particle sizes and packing densities. Nevertheless, we cannot exclude their effects.

In most cases, Cu with the same pore size exhibited better performance than CuO (cf. Fig. 6a and 6b) as metals are the typical active components for dry reforming reactions [42,58]. An exception is observed for the samples synthesized from the 1 μm silica spheres, i.e., the conversion of CuO-1000 is higher than of Cu-1000. These samples are also exceptions to the trend that the smaller the pore size, the better the performance. Indeed, these samples show a higher conversion in plasma-based dry reforming than both the smaller and larger pore size samples, and CuO-1000 even shows the highest conversion among all the unreduced CuO samples. We believe this can be attributed to the electric field enhancement in the pores with diameters close to the plasma Debye length (ca. 600 nm at typical plasma catalysis conditions) [39,40]. This electric field enhancement enables Cu-1000 and CuO-1000 to perform better than the other samples. Since mainly surface discharges occur in DBD plasma packed with materials with relatively low dielectric constant [42,58,70], such as CuO ($\epsilon_r = 18.1$), the electric field enhancement in this case due to surface charging is stronger than that of Cu-1000. Metals are in this context equivalent to a dielectric with infinite dielectric constant, and thus, the plasma will mainly be characterized by local filamentary microdischarges [42,58,70]. As samples with small pores can provide more and smaller discharge gaps for the local filamentary microdischarges, they are more favorable in Cu samples for the plasma reaction than the electric field enhancement of Cu-1000 [42,70]. The above factors together can explain why CuO-1000 shows the highest conversion of the unreduced CuO samples, while Cu-10 is the best among the reduced Cu samples.

Among the other macroporous samples with similar specific surface area, CuO-2000 showed better performance than CuO-600, while the performance of Cu-2000 is similar to that of Cu-600. This might also be because the discharge mode dominated by surface discharges in CuO is more in line with the simulation of plasma propagation in pores [40], which predicts that a larger pore size allows more electrons to enter. However, in case of metallic materials, the discharge mode (characterized by local filamentary micro-discharges) is different.

The selectivities of the main components formed in plasma-catalytic

dry reforming with the various 3D porous samples with different pore sizes are plotted in Fig. 7. The carbon and hydrogen mass balance (shown in Fig. S8) is not entirely 100%. Therefore, there might still be a few possible liquid products and carbon deposits attached to the catalyst and the reactor, as well as the presence of other gaseous products that were not calibrated in the gas chromatograph, which cannot be counted. As shown in Fig. 7a and Fig. 7c, syngas is the predominant product in all experiments, and the CO selectivity is always higher than that of H₂. When comparing the samples with different pore sizes, some products do not differ significantly in selectivity, while others do. Interestingly, the difference in selectivity appears to correlate with the conversion of the reactants. A rough trend seems to be that samples exhibiting higher CH₄ and CO₂ conversions also have higher syngas (CO and H₂) selectivities, but lower selectivities for some unsaturated hydrocarbons and oxygenated organics, such as ethylene, methanol, and ethanol. The selectivity decrease is most striking for the Cu-1000 and CuO-1000 samples, and may be caused by the enhanced electric field in the samples, causing a higher conversion due to the higher energy input, and apparently a lower selectivity to these unsaturated hydrocarbons and oxygenates, in line with literature [33,45]. The empty reactor had higher plasma power (see Table 2 below) due to the absence of packing material which may hinder the discharge, also following the above trend, which exhibited a relatively high syngas selectivity and a low unsaturated hydrocarbon and oxygenates selectivity. Besides the electric field enhancement, the reaction of radicals within the pores is another factor that might affect the selectivity [61,62]. The trends in selectivity for the various products are different, indicating a different impact of the pore size on the reaction paths of the radicals. For example, the selectivity towards acetylene is low in CuO-1000 but relatively high in CuO-10, although both of them show a high conversion of CO₂ and CH₄. Since CO is the predominant carbon-containing product, the carbon balance shown in Fig. S8 has a similar trend to the selectivity of CO. For example, among the copper samples, Cu-10 also has the highest sum of detectable carbon-containing products selectivities. However, the carbon balance of CuO-1000 is lower than that of other samples, although its CO selectivity is similar or even slightly higher than other samples. This indicates that more carbon deposits or other products not calibrated in the GC were generated during the dry reforming of this sample.

In order to study the stability of dry reforming performance and possible carbon deposition on the samples, long-time plasma DRM tests and TGA measurements were performed. As shown in Fig. S9, the performance of Cu-10 decreased slightly (1%–2%) after 12 h of testing, while the conversion of CH₄ and CO₂ of CuO-1000 did not change significantly (<1%). Fig. S10 shows the TGA data of CuO-1000 and Cu-10 after 12 h plasma dry reforming. The used CuO-1000 has a small weight loss (~0.1%) when heated to 800 °C in a 80 mL/min of O₂, indicating that there is little carbon deposition on its surface and it was not reduced by H₂ and CO products in plasma dry reforming, which may be due to the relatively low input energy in this study. The TGA data of the used Cu-10 were compared with that of fresh Cu-10, since the weight

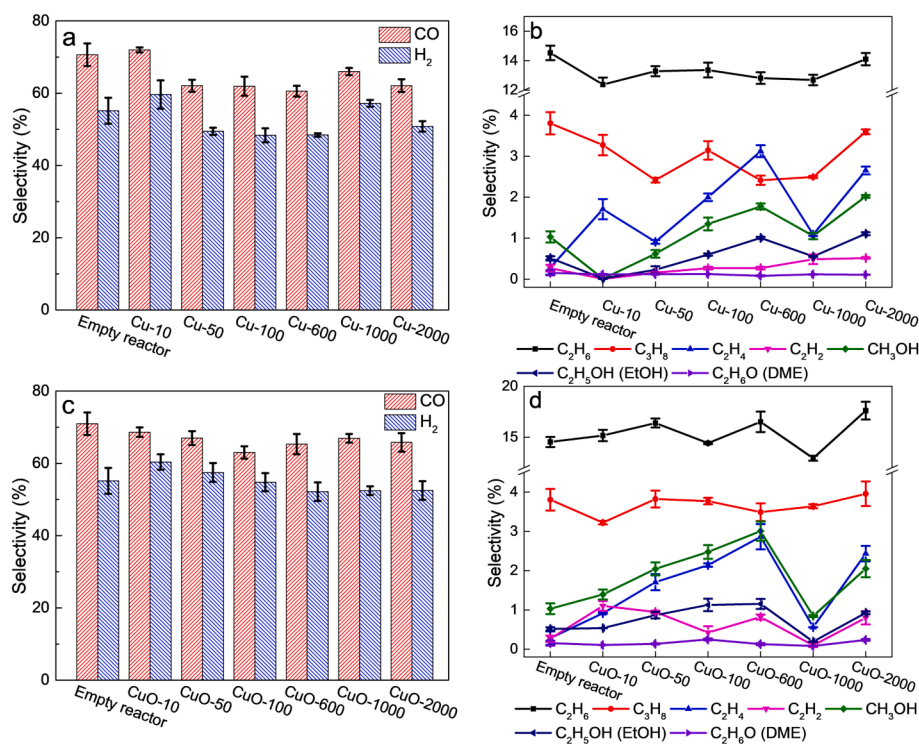


Fig. 7. Product selectivities in plasma-catalytic dry reforming, for CO and H₂ of 3D porous Cu (a) and CuO (c) samples with different pore sizes, and for ethane, propane, ethylene, acetylene, methanol, ethanol and dimethyl ether of 3D porous Cu (b) and CuO (d) samples with different pore sizes. The error bars were obtained from standard errors based on three repeats.

loss was covered by the weight increase caused by the oxidation of Cu. The weight difference after heating to 800 °C between the fresh Cu-10 and used Cu-10 was about 4.5%, which could be attributed to the carbon deposition from the 12 h plasma dry reforming, and this is also in line with its slightly reduced performance. In addition, as shown in Fig. S11, the reducibility of CuO-1000 did not change after the DRM test.

The electrical signals of the plasma experiments were recorded and collected by an oscilloscope. As seen in Table 2, 26–28 kV peak-to-peak voltage (U_{pp}) was applied to achieve a constant 50 W supplied power. However, depending on some factors, such as the structure and dielectric constant of the packing samples, at the same supplied power, the distribution, number and intensity of the discharges are different, resulting in different plasma powers. The portion of the supplied power that is not converted to plasma power is lost in the circuit as heat or returned to the source as reactive power. A higher plasma power, such as for the Cu-10, CuO-10, and CuO-1000 samples, means higher energy input, which produces a more reactive plasma, leading to their higher conversion. The higher plasma power in the empty reactor illustrates the hindering effect of the catalyst in the discharge, which should be one of the reasons why the conversion of most samples is lower than that in the empty reactor. The average number of micro-discharges per period is counted by the number of peaks in the normalized current profile after excluding signal noise. It may not be the exact number of micro-discharges, but subject to some system errors, as some discharges may coincide, or some may be too small and therefore are excluded as signal noise. By dividing the transferred charge by the number of micro-discharges in the same period, we obtain the average filament charge, which is a measure for the average strength of the discharge. Both a larger number of micro-discharges and more powerful discharges can have a positive effect on the conversion of plasma-based dry reforming. However, it is difficult for both to achieve relatively high values in the same reaction, since the catalyst pore size did not show a significant effect on the displaced charge. The displaced charge of the empty reactor could not be obtained due to the limited measurement range of the PC-

connected oscilloscope and the unstable discharge in the empty reactor. As shown in Table 2, a higher average filament charge often corresponds with fewer discharges, and exhibits higher conversion, cfr. Fig. 6. Therefore, our results suggest that the strength of the discharges has a larger effect on the conversion of plasma-based dry reforming than the number of micro-discharges.

However, most copper samples showed lower plasma power and discharge intensity than copper oxide with the same structure, despite they had a higher conversion of CO₂ and CH₄. The packing of the porous Cu powders in the reactor made some conductive particles to be directly connected to the grounded inner electrode to form an equipotential, which may cause most of the discharge to occur in the small gaps between the outermost particles (probably at the same potential as the electrode) and the dielectric barrier, and less point-to-point micro-discharges in the gaps between the other powders in the gap [42,58,70]. Although the reduced Cu has a negative impact on the discharge, they showed better performance in most cases than the CuO samples with higher plasma power and more produced radicals and ions, which might be due to its better catalytic activity for dry reforming. Fig. S12 shows the energy yields of the different samples, which exhibit the sample performance after normalizing for the difference in discharge power. The trend of EY variation with pore size is similar to that of conversion, further confirming the effect of pore size of the samples on the dry reforming performance. Since the discharge power of the Cu samples is always lower than that of the CuO samples, the performance advantage of Cu over CuO, shown by the EY, is larger than that shown by the conversion (except for Cu-1000 and CuO-1000). Since one of the reasons why the empty reactor has a higher conversion than most samples is its high discharge power, after excluding the influence of discharge power, two more samples, i.e., Cu-50 and Cu-1000, show better performance than the empty reactor, based on the EY.

4. Conclusion

In this study, we investigated the effect of catalyst pore size on plasma-based dry reforming. The samples evaluated in this study were 3D porous Cu or CuO, synthesized from uniform silica particles in the range of 10 nm to 2 μ m used as templates. Since the samples have similar pore structure, and consist of the same single chemistry without the interference of a support material, the plasma results can clearly show the influence of the catalyst pores in the plasma-based dry reforming.

Based on the conclusions drawn from previous simulation studies, we would expect that the larger the pore size, the better the catalyst performance, and the best results would be obtained for catalyst pore sizes above the plasma Debye length (hundreds of nanometers at typical plasma catalysis conditions [39,40]). That is because pores larger than the Debye length allow the plasma streamer to penetrate inside the catalyst pores and thus generate a larger contact area between plasma and catalyst surface for chemical reactions. However, our results do not reveal that the larger catalyst pore size is more favorable for the plasma reaction, but they show the opposite trend in most cases, with the exception of CuO-1000 (and Cu-1000 to some extent as well). This suggests that even when the electrons cannot enter the catalyst pores, because they are smaller than the Debye length, these pores can still be reached by radicals formed in the plasma, and ions can even be attracted into them due to the electric field, and these radicals and ions can give rise to the plasma-catalytic reactions. Among the reduced Cu samples, Cu-10 showed the highest conversion of CH₄ and CO₂, while among the CuO samples, CuO-1000 showed the highest conversion. We attribute the latter to the electric field enhancement, as predicted by modeling, as this pore size is close to the Debye length. The conversions of CH₄ and CO₂ of Cu-10 and CuO-1000 are higher than those of the empty reactor, indicating that the fully packing catalyst does not necessarily have a negative effect on the conversion as in the literature, and as long as it has a suitable structure, the conversions of CH₄ and CO₂ can be improved. Furthermore, a rough trend indicates that the higher the conversion of CH₄ and CO₂, the generally higher is the selectivity of syngas among the various products, and the lower is the selectivity of some unsaturated hydrocarbons and oxygenated organics. Finally, from the correlation with the electrical characteristics, we can conclude that the strength of the micro-discharges has an important effect on the conversion of CH₄ and CO₂ and the selectivity of the products, although there is no perfect correlation.

In the 3D porous samples synthesized by the template method, the thickness of the pore wall varies with the pore size, resulting in changes in the crystallite size of the components. Samples with larger pore sizes have larger crystallite size, which is detrimental to the conversion of dry reforming [66–69]. The difference in specific surface area for samples with pore sizes smaller than 100 nm and samples with larger pores is two orders of magnitude. Therefore, even if the plasma streamers can propagate into the large pores and react with the entire surface of the sample, which is not possible for the pores smaller than the Debye length, the total contact area with plasma will not rise a lot, and thus, it will not bring much improvement. On the other hand, even if plasma streamers cannot propagate in the smaller pores, as mentioned above, radicals or positively charged ions can still diffuse into these catalysts, and the latter even be attracted into it, and the effective contact area of these radicals and ions in small pores is much larger than for catalysts with larger pores.

In summary, we demonstrated that catalysts with smaller pores perform generally better for plasma-based dry reforming, but there are exceptions depending on the properties of the materials. The possible electric field enhancement due to surface charging in the large pores of a certain pore size can greatly improve the reaction efficiency. This enhancement effect is strong for CuO, which is characterized by a relatively small dielectric constant, while it is weak for metallic catalytically active components. Therefore, in future research of catalysts for plasma reactions, macroporous supports with specific pore size (possibly

several hundreds of nanometers) and metal active components with micropores (or the combination of both) are two potential feasible directions. This is not only for dry reforming, but could also be valid for more plasma-catalytic processes.

Declaration of Competing Interest

The authors declare that they have no known competing financial interests or personal relationships that could have appeared to influence the work reported in this paper.

Data availability

Data will be made available on request.

Acknowledgements

We acknowledge Prof. Anne-Marie De Wilde (VITO) for the Hg intrusion measurements, Gert Nuyts for the SEM measurements, Zhiyuan Cao and Quanzhi Zhang for their discussions of the experimental results. This work is supported by the China Scholarship Council (No. 201806060123); and the VLAIO Catalisti transition project CO2PERATE (HBC.2017.0692). K.Z acknowledges the EASiCHEM project funded by the Flemish Strategic Basic Research Program of the Catalisti cluster and Flanders Innovation & Entrepreneurship (HBC.2018.0484).

Appendix A. Supplementary data

Supplementary data to this article can be found online at <https://doi.org/10.1016/j.cej.2023.142574>.

References

- [1] A. Bogaerts, X. Tu, J.C. Whitehead, G. Centi, L. Lefferts, O. Guaitella, F. Azzolina-Jury, H.-H. Kim, A.B. Murphy, W.F. Schneider, T. Nozaki, J.C. Hicks, A. Rousseau, F. Thevenet, A. Khacef, M. Carreon, The 2020 plasma catalysis roadmap, *J. Phys. D Appl. Phys.* 53 (44) (2020) 443001.
- [2] Y. Yi, J. Zhou, H. Guo, J. Zhao, J. Su, L. Wang, X. Wang, W. Gong, Safe direct synthesis of high purity H₂O₂ through a H₂/O₂ plasma reaction, *Angew. Chem. Int. Ed.* 52 (2013) 8446–8449, <https://doi.org/10.1002/anie.201304134>.
- [3] Y. Yi, S. Li, Z. Cui, Y. Hao, Y. Zhang, L. Wang, P. Liu, X. Tu, X. Xu, H. Guo, A. Bogaerts, Selective oxidation of CH₄ to CH₃OH through plasma catalysis: insights from catalyst characterization and chemical kinetics modelling, *Appl. Catal. B Environ.* 296 (2021), 120384, <https://doi.org/10.1016/j.apcatb.2021.120384>.
- [4] Y. Song, E. Ozdemir, S. Ramesh, A. Adishev, S. Subramanian, A. Harale, M. Albuali, A. Fadhel Bandar, A. Jamal, D. Moon, H. Choi Sun, T. Yavuz Cafer, Dry reforming of methane by stable Ni–Mo nanocatalysts on single-crystalline MgO, *Science* 367 (2020) 777–781, <https://doi.org/10.1126/science.aav2412>.
- [5] C. Wang, Y. Wang, M. Chen, D. Liang, Z. Yang, W. Cheng, Z. Tang, J. Wang, H. Zhang, Recent advances during CH₄ dry reforming for syngas production: a mini review, *Int. J. Hydrogen Energy* 46 (2021) 5852–5874, <https://doi.org/10.1016/j.ijhydene.2020.10.240>.
- [6] L. Zhou, J.M.P. Martirez, J. Finzel, C. Zhang, D.F. Swearer, S. Tian, H. Robotjazi, M. Lou, L. Dong, L. Henderson, P. Christopher, E.A. Carter, P. Nordlander, N. J. Halas, Light-driven methane dry reforming with single atomic site antenna-reactor plasmonic photocatalysts, *Nat. Energy* 5 (2020) 61–70, <https://doi.org/10.1038/s41560-019-0517-9>.
- [7] C. Palmer, D.C. Upham, S. Smart, M.J. Gordon, H. Metiu, E.W. McFarland, Dry reforming of methane catalysed by molten metal alloys, *Nat. Catal.* 3 (2020) 83–89, <https://doi.org/10.1038/s41929-019-0416-2>.
- [8] H.U. Hambali, A.A. Jalil, A.A. Abdulrasheed, T.J. Siang, A.H.K. Owgi, F.F.A. Aziz, CO₂ reforming of methane over Ta-promoted Ni/ZSM-5 fibre-like catalyst: insights on deactivation behavior and optimization using response surface methodology (RSM), *Chem. Eng. Sci.* 231 (2021), 116320, <https://doi.org/10.1016/j.ces.2020.116320>.
- [9] L.C. Buelens, V.V. Galvita, H. Poelman, C. Detavernier, G.B. Marin, Super-dry reforming of methane intensifies CO₂ utilization via Le Chatelier's principle, *Science* 354 (2016) 449–452, <https://doi.org/10.1126/science.aah7161>.
- [10] M. Usman, W.M.A. Wan Daud, H.F. Abbas, Dry reforming of methane: Influence of process parameters—a review, *Renewable Sustainable Energy Rev.* 45 (2015) 710–744, <https://doi.org/10.1016/j.rser.2015.02.026>.
- [11] G. Zhang, J. Liu, Y. Xu, Y. Sun, A review of CH₄-CO₂ reforming to synthesis gas over Ni-based catalysts in recent years (2010–2017), *Int. J. Hydrogen Energy* 43 (2018) 15030–15054, <https://doi.org/10.1016/j.ijhydene.2018.06.091>.

- [12] N.A.K. Aramouni, J.G. Touma, B.A. Tarboush, J. Zeaiter, M.N. Ahmad, Catalyst design for dry reforming of methane: Analysis review, *Renewable Sustainable Energy Rev.* 82 (2018) 2570–2585, <https://doi.org/10.1016/j.rser.2017.09.076>.
- [13] R.S. Abiev, D.A. Sladkovskiy, K.V. Semikin, D.Y. Murzin, E.V. Rebrov, Non-thermal plasma for process and energy intensification in dry reforming of methane, *Catalysts* 10 (2020) 1358, <https://doi.org/10.3390/catal10111358>.
- [14] C. Shi, S. Wang, X. Ge, S. Deng, B. Chen, J. Shen, A review of different catalytic systems for dry reforming of methane: conventional catalysis-alone and plasma-catalytic system, *J. CO₂ Utilization* 46 (2021), 101462, <https://doi.org/10.1016/j.jcou.2021.101462>.
- [15] Z. Li, Q. Lin, M. Li, J. Cao, F. Liu, H. Pan, Z. Wang, S. Kawi, Recent advances in process and catalyst for CO₂ reforming of methane, *Renewable Sustainable Energy Rev.* 134 (2020), 110312, <https://doi.org/10.1016/j.rser.2020.110312>.
- [16] R. Snoeckx, A. Bogaerts, Plasma technology – a novel solution for CO₂ conversion? *Chem. Soc. Rev.* 46 (2017) 5805–5863, <https://doi.org/10.1039/C6CS00066E>.
- [17] B.S. Patil, N. Cherkasov, J.A.O. Ibhado, V. Hessel, Q. Wang, Low temperature plasma-catalytic NO_x synthesis in a packed DBD reactor: effect of support materials and supported active metal oxides, *Appl. Catal. B Environ.* 194 (2016) 123–133, <https://doi.org/10.1016/j.apcatb.2016.04.055>.
- [18] L. Wang, Y. Yi, C. Wu, H. Guo, X. Tu, One-step reforming of CO₂ and CH₄ into high-value liquid chemicals and fuels at room temperature by plasma-driven catalysis, *Angew. Chem. Int. Ed.* 56 (2017) 13679–13683, <https://doi.org/10.1002/anie.201707131>.
- [19] Y. Uytendhouwen, K.M. Bal, E.C. Neyts, V. Meynen, P. Cool, A. Bogaerts, On the kinetics and equilibria of plasma-based dry reforming of methane, *Chem. Eng. J.* 405 (2021), 126630, <https://doi.org/10.1016/j.cej.2020.126630>.
- [20] X. Tu, J.C. Whitehead, Plasma dry reforming of methane in an atmospheric pressure AC gliding arc discharge: Co-generation of syngas and carbon nanomaterials, *Int. J. Hydrogen Energy* 39 (2014) 9658–9669, <https://doi.org/10.1016/j.ijhydene.2014.04.073>.
- [21] Y. Yi, C. Xu, L. Wang, J. Yu, Q. Zhu, S. Sun, X. Tu, C. Meng, J. Zhang, H. Guo, Selectivity control of H₂/O₂ plasma reaction for direct synthesis of high purity H₂O₂ with desired concentration, *Chem. Eng. J.* 313 (2017) 37–46, <https://doi.org/10.1016/j.cej.2016.12.043>.
- [22] A.H. Khoja, M. Tahir, N.A.S. Amin, Dry reforming of methane using different dielectric materials and DBD plasma reactor configurations, *Energy Convers. Manage.* 144 (2017) 262–274, <https://doi.org/10.1016/j.enconman.2017.04.057>.
- [23] Y. Uytendhouwen, J. Herejigers, T. Breugelmanns, P. Cool, A. Bogaerts, How gas flow design can influence the performance of a DBD plasma reactor for dry reforming of methane, *Chem. Eng. J.* 405 (2021), 126618, <https://doi.org/10.1016/j.cej.2020.126618>.
- [24] F. Zhu, H. Zhang, X. Yan, J. Yan, M. Ni, X. Li, X. Tu, Plasma-catalytic reforming of CO₂-rich biogas over Ni/γ-Al₂O₃ catalysts in a rotating gliding arc reactor, *Fuel* 199 (2017) 430–437, <https://doi.org/10.1016/j.fuel.2017.02.082>.
- [25] M.-W. Li, G.-H. Xu, Y.-L. Tian, L. Chen, H.-F. Fu, Carbon dioxide reforming of methane using dc corona discharge plasma reaction, *J. Phys. Chem. A* 108 (2004) 1687–1693, <https://doi.org/10.1021/jp037008q>.
- [26] Y. Yi, X. Wang, A. Jafarzadeh, L. Wang, P. Liu, B. He, J. Yan, R. Zhang, H. Zhang, X. Liu, H. Guo, E.C. Neyts, A. Bogaerts, Plasma-catalytic ammonia reforming of methane over Cu-based catalysts for the production of HCN and H₂ at reduced temperature, *ACS Catalysis* 11 (2021) 1765–1773, <https://doi.org/10.1021/acscatal.0c04940>.
- [27] I. Michielsens, Y. Uytendhouwen, J. Pype, B. Michielsens, J. Mertens, F. Reniers, V. Meynen, A. Bogaerts, CO₂ dissociation in a packed bed DBD reactor: first steps towards a better understanding of plasma catalysis, *Chem. Eng. J.* 326 (2017) 477–488, <https://doi.org/10.1016/j.cej.2017.05.177>.
- [28] Y. Uytendhouwen, S. Van Alphen, I. Michielsens, V. Meynen, P. Cool, A. Bogaerts, A packed-bed DBD micro plasma reactor for CO₂ dissociation: does size matter? *Chem. Eng. J.* 348 (2018) 557–568, <https://doi.org/10.1016/j.cej.2018.04.210>.
- [29] Y. Uytendhouwen, K.M. Bal, I. Michielsens, E.C. Neyts, V. Meynen, P. Cool, A. Bogaerts, How process parameters and packing materials tune chemical equilibrium and kinetics in plasma-based CO₂ conversion, *Chem. Eng. J.* 372 (2019) 1253–1264, <https://doi.org/10.1016/j.cej.2019.05.008>.
- [30] B. Wang, M. Mikhail, S. Cavadias, M. Tatoulian, P. Da Costa, S. Ognier, Improvement of the activity of CO₂ methanation in a hybrid plasma-catalytic process in varying catalyst particle size or under pressure, *J. CO₂ Utilization* 46 (2021), 101471, <https://doi.org/10.1016/j.jcou.2021.101471>.
- [31] R. Vakili, R. Gholami, C.E. Stere, S. Chansai, H. Chen, S.M. Holmes, Y. Jiao, C. Hadraque, X. Fan, Plasma-assisted catalytic dry reforming of methane (DRM) over metal-organic frameworks (MOFs)-based catalysts, *Appl. Catal. B Environ.* 260 (2020), 118195, <https://doi.org/10.1016/j.apcatb.2019.118195>.
- [32] Y. Zeng, X. Zhu, D. Mei, B. Ashford, X. Tu, Plasma-catalytic dry reforming of methane over γ-Al₂O₃ supported metal catalysts, *Catal. Today* 256 (2015) 80–87, <https://doi.org/10.1016/j.cattod.2015.02.007>.
- [33] X. Tu, H.J. Gallon, M.V. Twigg, P.A. Gorry, J.C. Whitehead, Dry reforming of methane over a Ni/Al₂O₃ catalyst in a coaxial dielectric barrier discharge reactor, *J. Phys. D Appl. Phys.* 44 (27) (2011) 274007.
- [34] H.K. Song, J.-W. Choi, S.H. Yue, H. Lee, B.-K. Na, Synthesis gas production via dielectric barrier discharge over Ni/γ-Al₂O₃ catalyst, *Catal. Today* 89 (2004) 27–33, <https://doi.org/10.1016/j.cattod.2003.11.009>.
- [35] J. Sentek, K. Krawczyk, M. Mlotek, M. Kalczewska, T. Kroker, T. Kolb, A. Schenk, K.-H. Gericke, K. Schmidt-Szalowski, Plasma-catalytic methane conversion with carbon dioxide in dielectric barrier discharges, *Appl. Catal. B Environ.* 94 (2010) 19–26, <https://doi.org/10.1016/j.apcatb.2009.10.016>.
- [36] I. Michielsens, Y. Uytendhouwen, A. Bogaerts, V. Meynen, Altering conversion and product selectivity of dry reforming of methane in a dielectric barrier discharge by changing the dielectric packing material, *Catalysts* 9 (1) (2019) 51.
- [37] J.A. Andersen, J.M. Christensen, M. Østberg, A. Bogaerts, A.D. Jensen, Plasma-catalytic dry reforming of methane: Screening of catalytic materials in a coaxial packed-bed DBD reactor, *Chem. Eng. J.* 397 (2020), 125519, <https://doi.org/10.1016/j.cej.2020.125519>.
- [38] X. Tu, J.C. Whitehead, Plasma-catalytic dry reforming of methane in an atmospheric dielectric barrier discharge: Understanding the synergistic effect at low temperature, *Appl. Catal. B Environ.* 125 (2012) 439–448, <https://doi.org/10.1016/j.apcatb.2012.06.006>.
- [39] Q.-Z. Zhang, A. Bogaerts, Plasma streamer propagation in structured catalysts, *Plasma Sources Sci. Technol.* 27 (2018), 105013, <https://doi.org/10.1088/1361-6595/aae430>.
- [40] Q.-Z. Zhang, A. Bogaerts, Propagation of a plasma streamer in catalyst pores, *Plasma Sources Sci. Technol.* 27 (2018), 035009, <https://doi.org/10.1088/1361-6595/aab47a>.
- [41] Y.-R. Zhang, K. Van Laer, E.C. Neyts, A. Bogaerts, Can plasma be formed in catalyst pores? a modeling investigation, *Appl. Catal. B Environ.* 185 (2016) 56–67, <https://doi.org/10.1016/j.apcatb.2015.12.009>.
- [42] Q.-Z. Zhang, W.-Z. Wang, A. Bogaerts, Importance of surface charging during plasma streamer propagation in catalyst pores, *Plasma Sources Sci. Technol.* 27 (2018), 065009, <https://doi.org/10.1088/1361-6595/aaca6d>.
- [43] X. Zheng, S. Tan, L. Dong, S. Li, H. Chen, LaNiO₃@SiO₂ core-shell nano-particles for the dry reforming of CH₄ in the dielectric barrier discharge plasma, *Int. J. Hydrogen Energy* 39 (2014) 11360–11367, <https://doi.org/10.1016/j.ijhydene.2014.05.083>.
- [44] D. Ray, D. Nepal, T. Vinodkumar, C. Subrahmanyam, g-C₃N₄ promoted DBD plasma assisted dry reforming of methane, *Energy* 183 (2019) 630–638, <https://doi.org/10.1016/j.energy.2019.06.147>.
- [45] D. Ray, P.M.K. Reddy, C. Subrahmanyam, Ni-Mn/γ-Al₂O₃ assisted plasma dry reforming of methane, *Catal. Today* 309 (2018) 212–218, <https://doi.org/10.1016/j.cattod.2017.07.003>.
- [46] D. Ray, D. Nepal, S. Janampelli, P. Goshal, C. Subrahmanyam, Dry reforming of methane in DBD plasma over Ni-Based catalysts: influence of process conditions and support on performance and durability, *Energy Technol.* 7 (2019) 1801008, <https://doi.org/10.1002/ente.201801008>.
- [47] X. Gao, Z. Lin, T. Li, L. Huang, J. Zhang, S. Askari, N. Dewangan, A. Jangam, S. Kawi, Recent developments in dielectric barrier discharge plasma-assisted catalytic dry reforming of methane over Ni-based catalysts, *Catalysts* 11 (4) (2021) 455.
- [48] Q. Xie, S. Zhuge, X. Song, M. Lu, F. Yu, R. Ruan, Y. Nie, Non-thermal atmospheric plasma synthesis of ammonia in a DBD reactor packed with various catalysts, *J. Phys. D Appl. Phys.* 53 (6) (2020) 064002.
- [49] A.H. Khoja, M. Tahir, N.A.S. Amin, Recent developments in non-thermal catalytic DBD plasma reactor for dry reforming of methane, *Energy Convers. Manage.* 183 (2019) 529–560, <https://doi.org/10.1016/j.enconman.2018.12.112>.
- [50] J. Wang, K. Zhang, S. Kavak, S. Bals, V. Meynen, Modifying the stöber process: is the organic solvent indispensable? *Chem. – A European J. n/a* (2022) <https://doi.org/10.1002/chem.202202670>.
- [51] J. Van Turnhout, D. Aceto, A. Travert, P. Bazin, F. Thibault-Starzyk, A. Bogaerts, F. Azzolina-Jury, Observation of surface species in plasma-catalytic dry reforming of methane in a novel atmospheric pressure dielectric barrier discharge in situ IR cell, *Catal. Sci. Technol.* 12 (2022) 6676–6686, <https://doi.org/10.1039/D2CY00311B>.
- [52] N. Pinhão, A. Moura, J.B. Branco, J. Neves, Influence of gas expansion on process parameters in non-thermal plasma plug-flow reactors: a study applied to dry reforming of methane, *Int. J. Hydrogen Energy* 41 (2016) 9245–9255, <https://doi.org/10.1016/j.ijhydene.2016.04.148>.
- [53] Y. Zhang, B. Yang, Z. Yang, G. Ye, Ink-bottle effect and pore size distribution of cementitious materials identified by pressurization-depressurization cycling mercury intrusion porosimetry, *Materials* 12 (9) (2019) 1454.
- [54] F. Moro, H. Böhm, Ink-bottle effect in mercury intrusion porosimetry of cement-based materials, *J. Colloid Interface Sci.* 246 (2002) 135–149, <https://doi.org/10.1006/jcis.2001.7962>.
- [55] R.P. Mayer, R.A. Stowe, Mercury porosimetry—breakthrough pressure for penetration between packed spheres, *J. Colloid Sci.* 20 (1965) 893–911, [https://doi.org/10.1016/0095-8522\(65\)90061-9](https://doi.org/10.1016/0095-8522(65)90061-9).
- [56] H.K. Palmer, R.C. Rowe, The application of mercury porosimetry to porous polymer powders, *Powder Technol.* 9 (1974) 181–186, [https://doi.org/10.1016/0032-5910\(74\)80030-6](https://doi.org/10.1016/0032-5910(74)80030-6).
- [57] J. Feng, W. Mo, S. Ma, Y. Wang, J. Yang, X. Su, G. Wang, M. Lin, Thermal shrinkage inhibition mechanism of fumed silica based thermal insulating composite, *Appl. Therm. Eng.* 113 (2017) 749–755, <https://doi.org/10.1016/j.applthermaleng.2016.11.081>.
- [58] A. Bogaerts, Q.-Z. Zhang, Y.-R. Zhang, K. Van Laer, W. Wang, Burning questions of plasma catalysis: Answers by modeling, *Catal. Today* 337 (2019) 3–14, <https://doi.org/10.1016/j.cattod.2019.04.077>.
- [59] S. Kameshima, R. Mizukami, T. Yamazaki, L.A. Prananto, T. Nozaki, Interfacial reactions between DBD and porous catalyst in dry methane reforming, *J. Phys. D Appl. Phys.* 51 (11) (2018) 114006.
- [60] K. Hensel, S. Katsura, A. Mizuno, DC microdischarges inside porous ceramics, *IEEE Trans. Plasma Sci.* 33 (2005) 574–575, <https://doi.org/10.1109/TPS.2005.845389>.

- [61] R. Snoeckx, R. Aerts, X. Tu, A. Bogaerts, Plasma-based dry reforming: a computational study ranging from the nanoseconds to seconds time scale, *J. Phys. Chem. C* 117 (2013) 4957–4970, <https://doi.org/10.1021/jp311912b>.
- [62] B. Loenders, Y. Engelmann, A. Bogaerts, Plasma-catalytic partial oxidation of methane on pt(111): a microkinetic study on the role of different plasma species, *J. Phys. Chem. C* 125 (2021) 2966–2983, <https://doi.org/10.1021/acs.jpcc.0c09849>.
- [63] E.C. Neyts, A. Bogaerts, Understanding plasma catalysis through modelling and simulation—a review, *J. Phys. D Appl. Phys.* 47 (22) (2014) 224010.
- [64] K. Woo Seok, P. Jin Myung, K. Yongho, H. Sang Hee, Numerical study on influences of barrier arrangements on dielectric barrier discharge characteristics, *IEEE Trans. Plasma Sci.* 31 (2003) 504–510, <https://doi.org/10.1109/TPS.2003.815469>.
- [65] O. Tilmatine, L. Dascalescu, T. Zeghloul, K. Medles, A. Fatu, Study of the influence of the different parameters of the atmospheric dbd treatment on the surface roughness and the electric potential distribution generated after the tribocharging of polypropylene, *IEEE Trans. Ind. Appl.* 57 (2021) 4162–4169, <https://doi.org/10.1109/TIA.2021.3081607>.
- [66] N. Rahemi, M. Haghghi, A.A. Babaluo, M.F. Jafari, S. Khorram, Non-thermal plasma assisted synthesis and physicochemical characterizations of Co and Cu doped Ni/Al₂O₃ nanocatalysts used for dry reforming of methane, *Int. J. Hydrogen Energy* 38 (2013) 16048–16061, <https://doi.org/10.1016/j.ijhydene.2013.08.084>.
- [67] I. Luisetto, S. Tuti, C. Battocchio, S. Lo Mastro, A. Sodo, Ni/CeO₂-Al₂O₃ catalysts for the dry reforming of methane: The effect of CeAlO₃ content and nickel crystallite size on catalytic activity and coke resistance, *Appl. Catal. A: Gen.* 500 (2015) 12–22, <https://doi.org/10.1016/j.apcata.2015.05.004>.
- [68] R.O. da Fonseca, A.R. Pongeggi, R.C. Rabelo-Neto, R.C.C. Simões, L.V. Mattos, F. B. Noronha, Controlling carbon formation over Ni/CeO₂ catalyst for dry reforming of CH₄ by tuning Ni crystallite size and oxygen vacancies of the support, *J. CO₂ Utilization* 57 (2022), 101880, <https://doi.org/10.1016/j.jcou.2021.101880>.
- [69] F. Mirzaei, M. Rezaei, F. Meshkani, Coprecipitated Ni-Co bimetallic nanocatalysts for methane dry reforming, *Chem. Eng. Technol.* 37 (2014) 973–978, <https://doi.org/10.1002/ceat.201300729>.
- [70] W. Wang, H.-H. Kim, K. Van Laer, A. Bogaerts, Streamer propagation in a packed bed plasma reactor for plasma catalysis applications, *Chem. Eng. J.* 334 (2018) 2467–2479, <https://doi.org/10.1016/j.cej.2017.11.139>.